

# Relationships between Ocean Bottom Noise and the Environment

by Jeffrey M. Babcock, Barry A. Kirkendall, and John A. Orcutt

**Abstract** Observations of ocean bottom low-frequency noise and surface environmental data over a period of 27 days in the northern Atlantic during the SAMSON and SWADE experiments reveal how closely related the noise is to meteorological conditions. Double-frequency microseisms produced by nonlinear interactions of storm-induced surface gravity waves are especially evident in the frequency band 0.16 to 0.3 Hz and show a high variability in both amplitude and peak frequencies. Bifurcated at times, the peak that characterizes the microseism band contains local and distant or “teleseismic” components, which are generated at different locations. Weather and storm fetch appear to be the major contributions to the size and shape of microseism spectra. Storm development on the sea surface is associated with progressively lower microseism frequencies along with a concurrent increase in amplitude. The single-frequency microseism peak is a continuous feature and is observed to portray the same time-dependent spectral characteristics as the portion of the double-frequency peak associated with distant storms. Coherence studies confirm that both peaks (single and teleseismic double) originate at a distant source. These peaks are generated at roughly the same location with some storm component over the coastline.

## Introduction

Though seafloor seismic and acoustic noise studies in the past have attempted to link large-scale environmental parameters to excitation of microseisms, a complete on-site coverage of surface conditions with concurrent ocean bottom measurements has not been accomplished, particularly in a deep ocean environment. Exceptions are those studies conducted near coastlines, which potentially yield results particular to a shallow water environment where local effects can dominate seafloor noise. The Office of Naval Research (ONR) Sources of Ambient Microseismic Ocean Noise (SAMSON) experiment was conducted in October–November 1990 off the coast of North Carolina to develop a synoptic view of low-frequency (0.01 to 2 Hz) ocean noise excitation and propagation (Fig. 1). In order to understand the effects of ocean-atmosphere coupling, the experiment was conducted in coordination with the ONR Surface Wave Dynamic Experiment (SWADE), which provided detailed meteorological and wave dynamics data. The SAMSON experiment, in conjunction with the SWADE experiment, provides an opportunity to comprehend fully the relationships between surface conditions and microseismic excitation for an open ocean setting.

Since different physics govern distinct parts of the microseism spectrum, a discussion of sources of seafloor noise is most conveniently broken into four frequency

bands. Typical pressure power spectra, collected from SAMSON, for frequencies spanning  $\sim 0.008$  to 4 Hz are shown in Figure 2. Successive spectral estimates are offset by an order of magnitude for a clearer display of spectral features. Though the data shown are particular to this experiment, measurements from different locations and environmental conditions show quite similar characteristics. Individual parts of the spectra are identified as follows:

- (A) Long-period surface gravity waves are characterized by high noise levels below  $\sim 20$  mHz, which are thought to be caused by long waves generated at the shoreline, called “surf beat” by Munk (1949) and Tucker (1950). Long waves generated in this band are mainly trapped as edge waves along the shore (Guza and Thornton, 1982; Symonds *et al.*, 1982), but some wave energy can escape to the deep sea by scattering from shoreline irregularities and other processes.
- (B) The “noise notch,” spanning roughly 20 to 100 mHz, reveals a rapid fall-off in power, and the level is thought to be controlled largely by currents and turbulence in the seafloor boundary layer (e.g., Webb, 1988; Orcutt *et al.*, 1993).
- (C) Though poorly understood, the “single frequency” or “primary frequency” microseism peak usually oc-

curs near 0.1 Hz. These microseisms are thought to be developed primarily in shallow water (e.g., Haubrich and McCamy, 1969; Cessoro and Chan, 1989), and a possible source involves breaking waves at the coast-line.

- (D) The “microseism peak” or “double-frequency microseism peak” is observed around 0.16 to 0.3 Hz and is excited by the nonlinear interaction between surface wind waves propagating in opposite directions (Longuet-Higgins, 1950; Hasselmann, 1963).
- (D’) The distant or “teleseismic” contribution to the microseism peak caused by distant storms is commonly observed at slightly lower frequencies.
- (E) The high-frequency end is characterized by a rapid

fall-off in power, where significant energy is associated with the interaction of higher-frequency surface wind waves generated by local wind activity.

This study is intended to assess the noise level change, especially in the double-frequency microseism band, that can be expected as a result of the influence of local meteorological conditions. The double-frequency peak is observed to be a very prominent feature and varies quite rapidly in amplitude and frequency throughout the experiment. Continuous recording over a period of 27 days allowed the temporal response of several large storms to be correlated with observed microseism activity. Also observed are the effects of distant weather-related sources

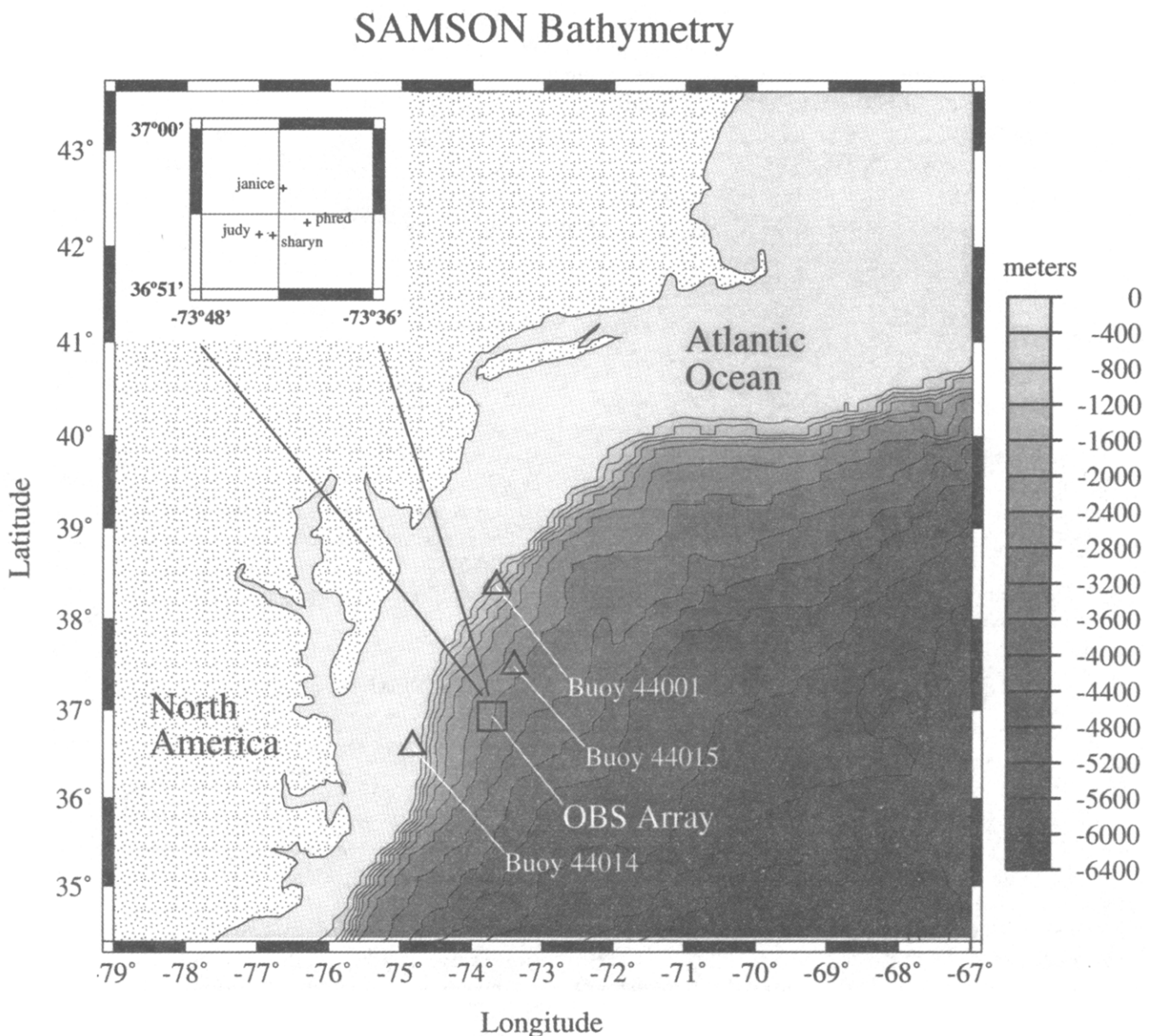


Figure 1. Bathymetry and locations of the three SWADE buoys and the SAMSON OBS array. Contours indicate depth in meters.

and the data provide clues that allow distant sources to be distinguished from local activity. Though seen only sporadically in many experiments conducted in the Pacific (Hedlin and Orcutt, 1989; Webb and Constable, 1986; Webb, 1992), the single-frequency peak was a continuous feature during this experiment, which provided a good opportunity to study its origin and propagation. Coherence studies make it possible to distinguish between microseisms generated at local and distant sources and reveal some of the interrelationships between different parts of the noise spectrum. Finally, a brief analysis of array studies gives insights into the modes of propagation for microseisms in the Atlantic Ocean.

### Theory

The most widely accepted mechanism for the excitation of microseisms involves the nonlinear interaction of opposing wave trains of surface gravity waves. In his classical analysis of microseism ground motion, Longuet-Higgins (1950) calculated the nondecaying pressure field arising from a standing gravity-wave field as a second-order effect. Hasselmann (1963) treated the excitation problem statistically and derived an expression for

the spectrum of a wave-induced pressure field and discussed the effects on seismic wave propagation. These early studies set the foundation for more extensive microseism research. Rather than reiterate the details of studies done by a multitude of researchers over the past several decades, a simplified overview of the theory behind microseism excitation and propagation is given.

Kibblewhite and Wu (1991), in a review article on excitation mechanisms, discuss and dismiss recent papers disputing wave-wave interactions as the primary source of microseisms in the band from 0.1 to 5 Hz. They also show that, for frequencies of present interest, nonlinear wave interactions of order higher than 2 will make little contribution to the noise-pressure field. Orcutt *et al.* (1993) give an interesting geometrical representation in three-dimensional  $\omega$ - $k$  space of a pair of interacting vectors, signifying surface gravity waves, that explains the conditions/cases in which a resultant acoustical wave can be induced. The wave-wave mechanism inferred is a nonlinear sum interaction that sums or doubles the frequencies of the waves and sums opposing wavenumbers for a near-zero wavenumber, high-phase-velocity acoustic wave. At microseism frequencies (0.01 to 4 Hz), the oceanic wave guide, bounded above by a pressure release surface and below by the rapid rise in

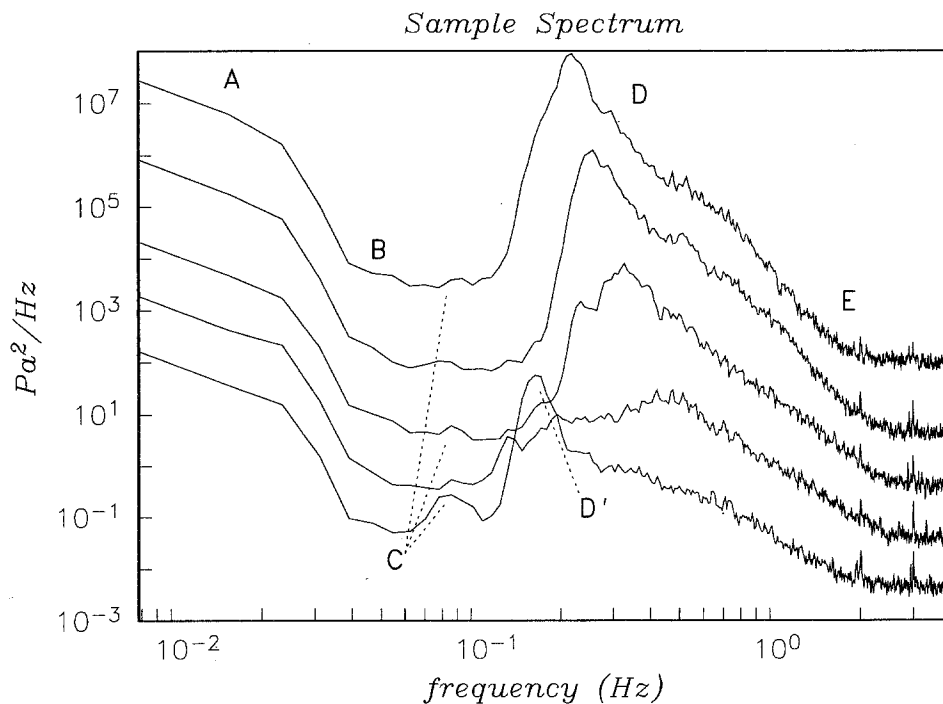


Figure 2. Sample spectra recorded during the SAMSON experiment. Successive spectral estimates are offset by an order of magnitude for clarity. Individual parts of the spectrum include the following: (A) ultra-low frequencies below  $\sim 20$  mHz, (B) the "noise notch," roughly spanning 20 to 100 mHz, (C) the "single" or "primary" frequency peak, usually occurring near 0.1 Hz, (D) the "double-frequency microseism peak" is observed around 0.16 to 0.3 Hz, (D') the distant or "teleseismic" contribution to the double-frequency microseism peak, and (E) the high-frequency end.

elastic wave velocities with depth beneath the seafloor, is efficient at propagating this acoustic energy generated at the sea surface. For microseism and lower frequencies, such an acoustic/elastic structure supports not only body waves but also surface waves as significant energy propagates below the seabed. Though not directly excited by the aforementioned interaction mechanism, interface or Stoneley modes are additionally produced through the coupling of surface-generated noise by sources, such as topography, close (less than a wavelength) to the ocean bottom interface (e.g., Schreiner and Dorman, 1990). Phase-velocity dispersion curves for simple ocean models outline high-velocity Rayleigh waves associated with crustal and uppermost mantle propagation, acoustic waves with a velocity very near 1.5 km/sec, and Stoneley modes with phase velocities very near zero (Orcutt *et al.*, 1993; Webb, 1992).

Hasselmann (1963) showed how the ocean wave spectrum could be used to predict the excitation of microseisms. Thus, in order to understand fully the generating mechanism, and predict microseismic activity, an understanding of the ocean surface wave spectrum is needed. It is widely known that the frequency of the main energy peak in the spectrum of surface gravity waves depends on the fetch and the wind speed. The waves grow until the phase velocity, which is inversely proportional to the frequency, equals that of the wind. Most models show the ocean surface wave spectrum maintains a constant and narrow bandwidth shape under increasing wind (Fig. 3). The Pierson and Moskowitz (1964) spec-

trum is shown here and gives an accurate representation for a "fully developed sea." Though more recent models, such as the JONSWAP spectrum (Hasselmann *et al.*, 1973), more accurately predict a narrower peak associated with lower-frequency waves and give a better description of the spectrum in regions of limited fetch, the overall shape and characteristics are quite similar. Of importance to this study is the general response of the wave spectra to different wind velocities. This will enable us to make a correlation between a temporal change in environmental conditions and excitation in the microseism band. Figure 3 shows how the wave spectrum evolves with increasing wind velocity as energy is transferred to lower-frequency, higher-amplitude components. At higher frequencies, the amplitude of the spectrum remains nearly unchanged or "saturated" for a variety of wind speeds. These basic features can also be observed in the microseism spectrum at frequencies roughly twice those shown in the wave spectrum (Fig. 4). Obviously, the wind plays a key role in determining the size and shape of microseisms. A saturated shape for the ocean wave spectrum appears to predict a saturated shape to the microseism spectrum (e.g., Webb, 1992). Knowledge of wind direction (and thus wave directional spectrum) is also an important contributing factor in microseism development and will be discussed in later sections.

#### Data and Observations

Four Ocean Bottom Seismographs (OBS's) recorded seafloor data on the continental slope off the coast of

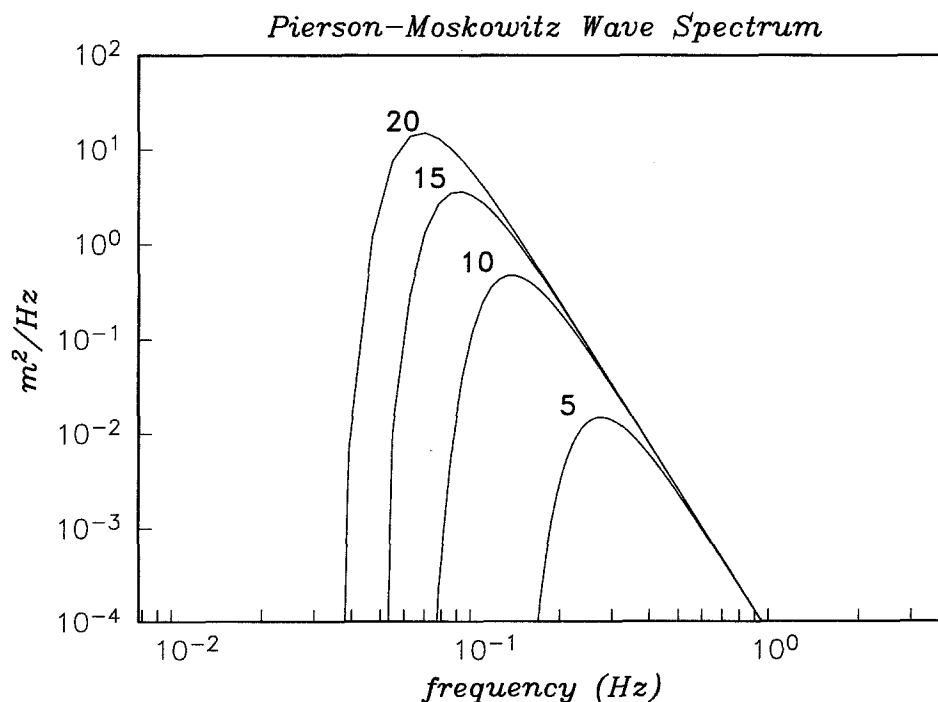


Figure 3. The Pierson and Moskowitz (1964) wave height spectrum for a fully developed sea under wind velocities of 5, 10, 15, and 20 m/sec.

North Carolina at an average depth of  $\sim 2622$  m and an aperture near 10 km from 18 October to 14 November 1990 (Fig. 1). Three SWADE buoys, each with an anchor to the seafloor, which floated on the surface of the water column in an array much larger than that of SAMSON, are also shown. The SWADE instruments recorded environmental data that were used to correlate surface conditions to ocean bottom excitation. Each instrument of the OBS array consisted of a single spherical pressure case containing microprocessor-based electronics, including three self-leveling geophones (two horizontal and one vertical) with a 1-Hz natural period, and a differential pressure gauge responsive to acoustic signals between 0.003 and 30 Hz (Willoughby *et al.*, 1993). Six instruments were originally deployed, of which four (named Janice, Judy, Phred, and Sharyn) recorded continuous data at a 32-Hz sampling rate throughout the entire experiment.

Several of the OBS's were found to have small 1-sec "tick marks" in the hydrophone data caused by an instrument noise problem in which a 1-Hz clock pulse fed into the preamplifier at a low level. This caused considerable contamination in the power spectrum at integer frequencies (i.e., 1, 2, 3, ... Hz). In an effort to remove the tick marks, the general form of the pulse was isolated by averaging 1 hr of 1-sec windows (3600 separate, 32 sample windows) and subsequently subtracting this waveform from the original data. This approach was very effective and visual examination of spectra before and

after this algorithm was applied revealed no significant alteration to the data except at integer frequencies.

Power spectral estimates were obtained over 1-hr periods using the Welch method of power spectral estimation (Oppenheim and Schaffer, 1975). Here, 28 nonoverlapping successive sections were Hanning windowed, transformed with a 4096-point FFT, and accumulated. This procedure was used in an effort to stabilize the spectral estimates, spanning 0.0078125 to 16 Hz and giving each frequency value approximately 56 degrees of freedom. Seismometer and pressure gauge power estimates have been corrected for instrument response. Coherence function estimates were calculated in a similar manner (28 4096-point sections) using data from every other hour. Values were computed by calculating the magnitude of the cross spectrum divided by the square root of the product of the autospectra.

### SWADE

Comparisons between available environmental data for the three SWADE instruments are shown in Figure 5. The buoys are located in the open ocean several hundred kilometers off the coast and, therefore, measurements have a very large "potential" fetch. Though the wind may not blow along the entire potential fetch, wind blowing over greater distances (usually from larger storms) is necessary to produce longer-period surface gravity waves leading to the generation of lower-frequency microseismic noise.

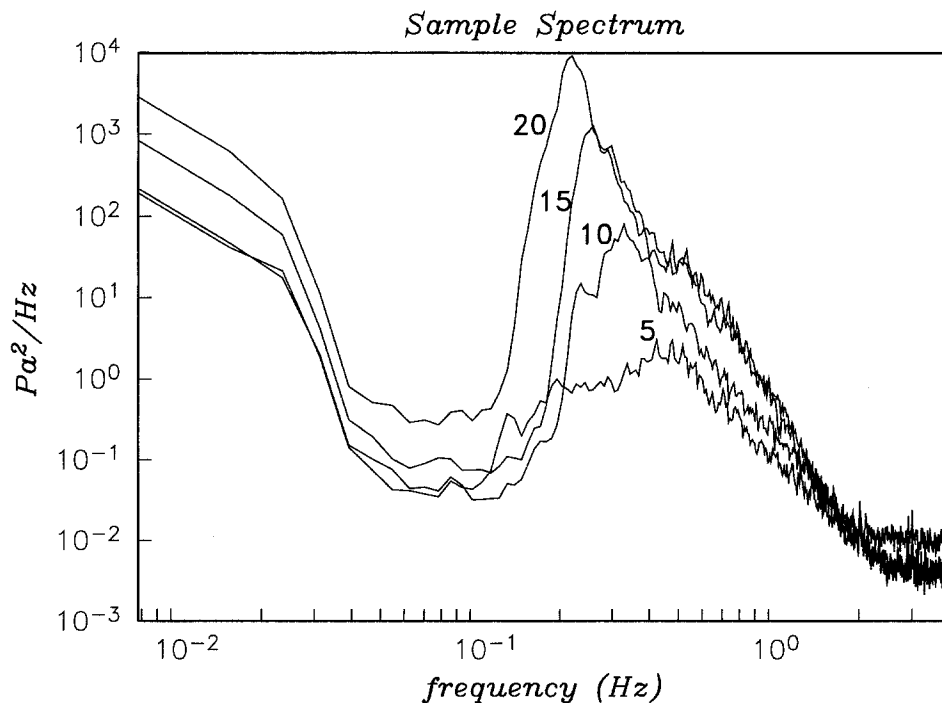


Figure 4. The same sample spectra shown in Figure 2 (excluding the bottom spectral estimate) plotted on a common amplitude scale without any offset. Wind velocities in meters per second are shown for each hour-long spectral estimate.

Significant events reported during the OBS deployment period include the following: (1) A southeast to north wind shift on day 292 (19 October), and (2) A nor'easter centered around day 299 (26 October). These features are readily visible in the data, especially the large nor'easter, which produced the highest wind velocities (over 20 m/sec) and included the largest significant wave heights (greater than 8 m). Also shown, but not reported, is a smaller event preceding the nor'easter close to day 297, as well as a series of storms toward the end of the experiment beginning near day 310. A more subtle feature is the relatively quiet meteorological period roughly spanning days 305 through 310. This lull in surface activity proved to be important in distinguishing between local and distant energy contributions to the microseism peak. Figure 6 shows the output from the vertical seismometer of OBS Phred for the entire recording period. There is a very good correlation between increases in

recorded noise levels and the weather features described above. As expected, the highest noise levels occur during the larger storms, such as the nor'easter, and the quiet meteorological period produced the lowest levels in the seismometer amplitude. Note: the spikes in the data are generally associated with earthquakes.

#### SWADE versus OBS

General comparisons revealing the interrelationships between surface environmental data (buoy 44015) and power spectral data from the vertical seismometer of OBS Janice are plotted in Figure 7. In the top frame the power levels at 0.20 Hz were chosen because this frequency approximately represents the center of the double-frequency peak. Increases in noise at this frequency must be attributed to increased nonlinear ocean wave interactions that generate propagating seismo-acoustic noise at small wavenumbers. Power levels here appear to vary

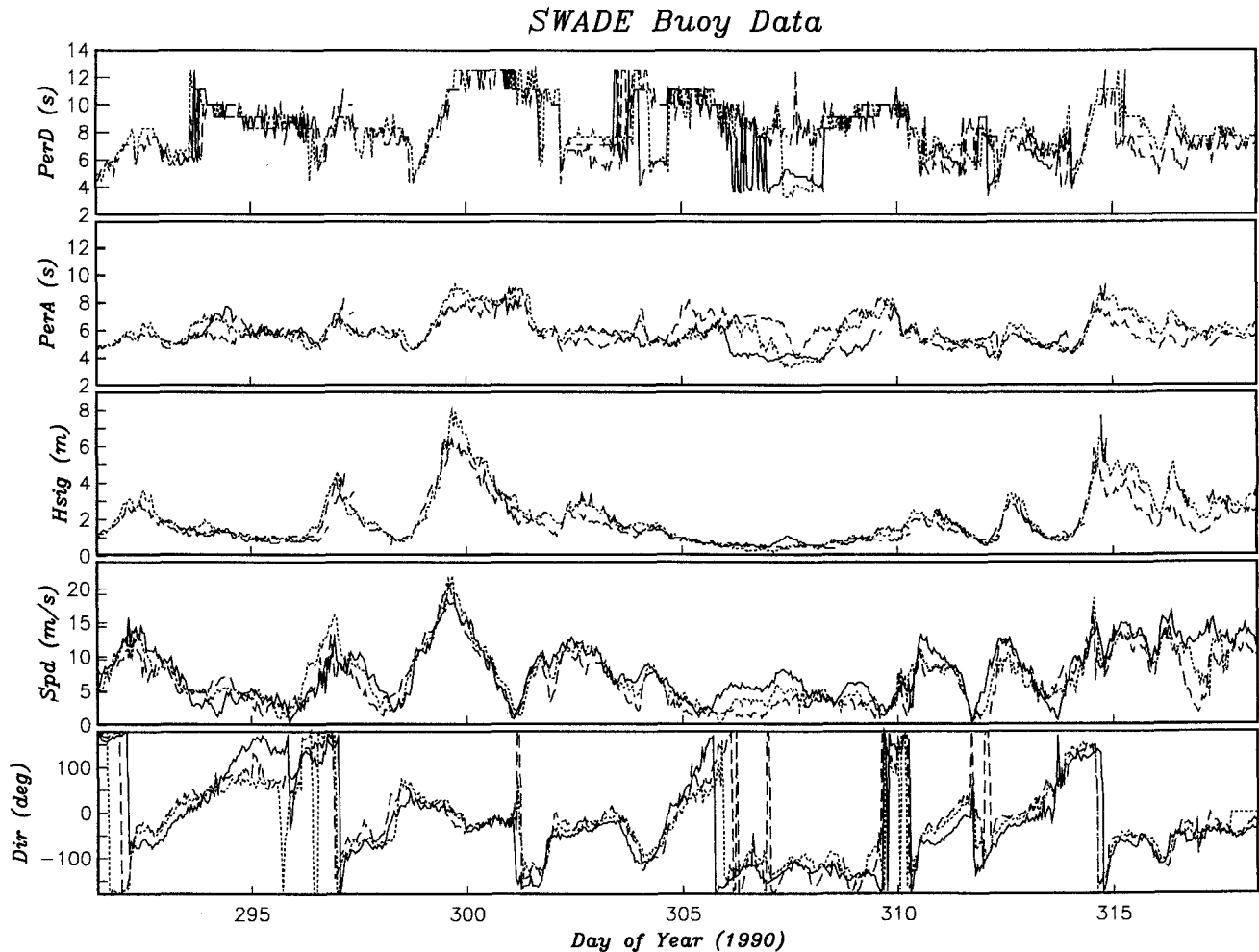


Figure 5. Comparisons between available environmental data for the three SWADE instruments. Buoys 44001 (solid), 44014 (dash), and 44015 (dot) show very similar results. Individual panels represent (from top to bottom) the dominant wave period (PerD), average wave period (PerA), significant wave height (Hsig), wind speed (Spd), and wind direction (Dir).

by as much as 4 orders of magnitude (40 dB). The second frame from the top shows the period at which the maximum power occurs for Janice. In the double-frequency band, the wind speed, wave height, and noise level at 0.2 Hz are clearly correlated. More evident at times when the wind is blowing hard, the periods of surface gravity waves and microseisms are seen to differ by roughly a factor of 2. Using the large nor'easter event (near day 300) as an example, increases in wave height tend to lag increases in wind velocity, which, in turn, are closely followed by higher noise levels at 0.2 Hz. At the same time, there is a shift from shorter- to longer-period surface gravity waves (higher to lower frequencies) and, subsequently, this same trend appears in the peak power levels of the microseism spectrum. Within the microseism peak, the three inertial components (channels 1, 2, and 3) and the hydrophone (channel 4) power levels at 0.2 Hz are highly correlated, as shown in Figure 8. In addition, the spectral amplitudes on the vertical and horizontal components are essentially identical. Figure 9 is a plot of the hydrophone channels for

the four operating OBS's and, again, the behavior is identical throughout the array, including the power levels recorded at 0.2 Hz.

Effects from abrupt changes in wind direction are especially evident. As reported, there is an abrupt wind shift associated with the first weather event (day 292), which causes power levels at 0.2 Hz to be somewhat elevated while similar events, with comparable wind velocities and significant wave heights (such as the small storm near day 313), reveal lower relative microseism amplitudes (see Fig. 7). This discrepancy can be explained by a shift toward a more isotropic directional spectrum for surface gravity waves in response to veering and unsteady winds (i.e., a wind shift produces surface gravity waves traveling in many different directions). This enables more waves of opposing wavenumber to interact and, therefore, higher relative microseismic amplitudes are predicted (Webb, 1992). Somewhat unexpectedly, the microseism peak period increases to 6 sec during the span of the quiet meteorological period (days 305 through 310). In fact, during this period, it

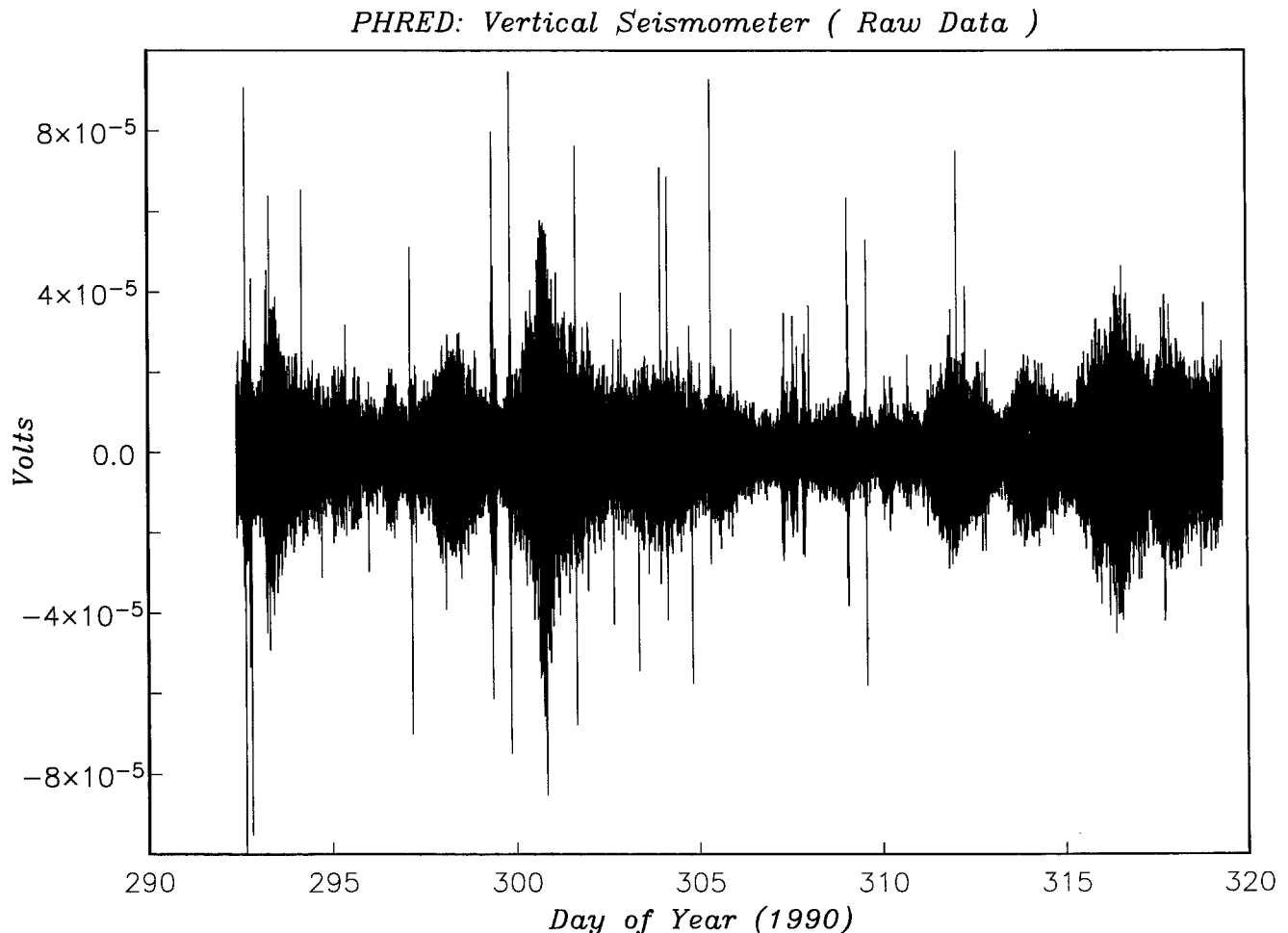


Figure 6. Output from the vertical seismometer of OBS Phred over the entire recording period. Higher relative noise levels occur during storms. The spikes in the data are generally associated with earthquakes.

appears that the microseisms are propagating into the area from afar, and the local contribution is minimal. These distant or teleseismic contributions also explain the elevated amplitudes observed during the environmental quiet period (see Fig. 7).

### Discussion

#### The Double Frequency Peak

A contoured power spectrum (spectrogram) for the vertical seismometer of Janice versus time and spanning the entire experiment is shown in Figure 10. The double-frequency peak can be seen centered near 0.2 Hz. Here, the small black circles represent the frequency at which the maximum power occurs in the microseism peak. This plot is particularly good for showing the response due to

the passage of a storm. Focusing on the first storm near the beginning of the experiment (day 292), there is a distinct migration from higher to lower frequencies, with a concurrent increase in power levels. As previously discussed, these are the same characteristics that occur in predicted surface gravity wave and microseism spectra. This trend corresponds to the increasing wind speed at the onset of the storm, which first generates smaller-amplitude, higher-frequency surface gravity waves and consequently excites the higher-frequency microseisms. As the storm progresses, the higher sustained winds produce higher-amplitude, lower-frequency surface waves, as well as microseism noise. A more detailed discussion of wind-wave growth and subsequent ocean wave spectral models is given by Hasselmann *et al.* (1973) and by Pierson and Moskowitz (1964) for fully developed seas.

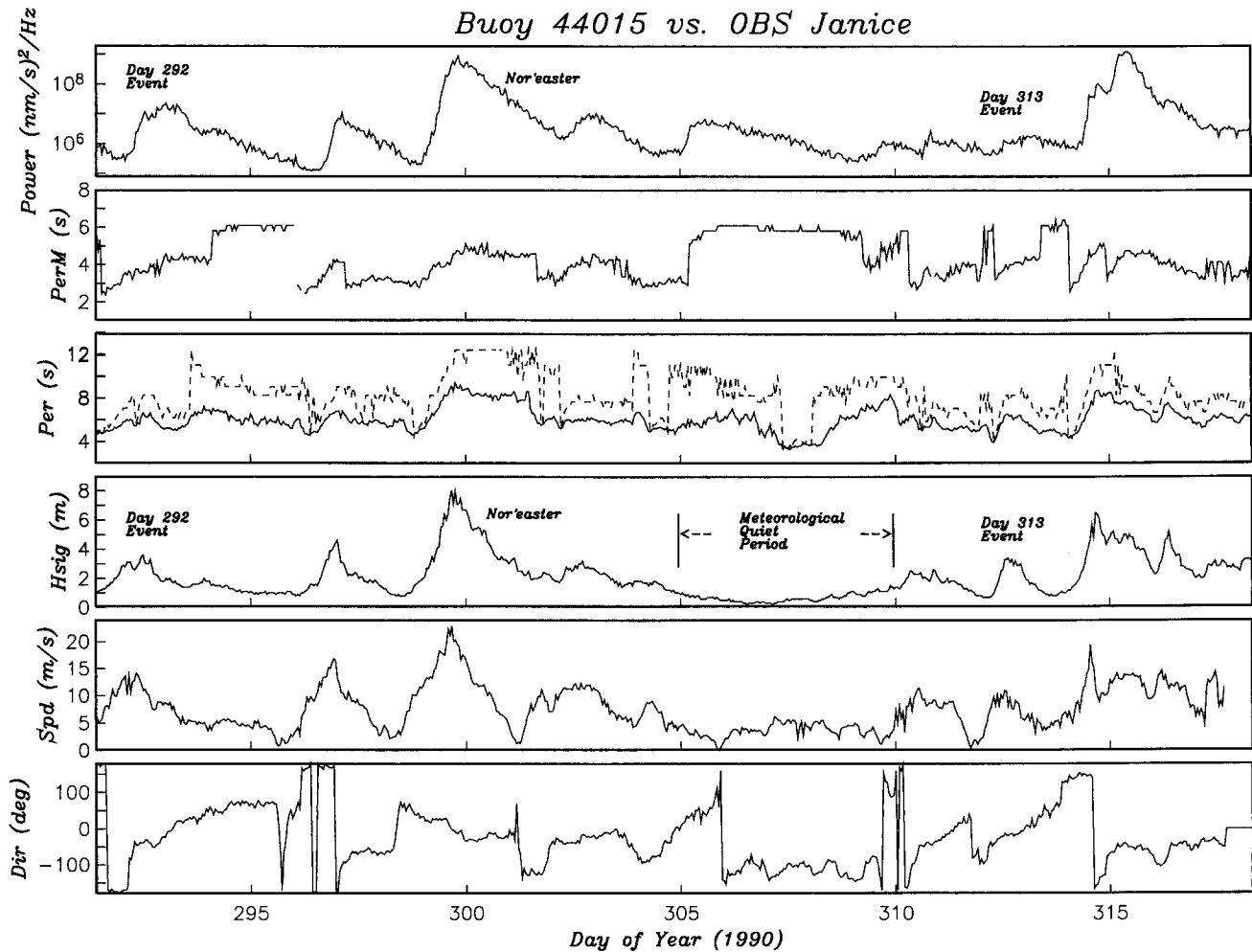


Figure 7. General comparisons between meteorological and microseism data. Buoy 44015 is shown here because it is closest to the OBS array. Individual panels represent (from top to bottom) the power spectral level at 0.20 Hz from the vertical seismometer of OBS Janice (Power), the period at maximum power for Janice's vertical seismometer (PerM), average (solid) and dominant (dash) wave periods for Buoy 44015 (Per), significant wave height (Hsig), wind speed (Spd), and wind direction (Dir).

In another example, the large nor'easter event (near day 300) reveals a similar reaction in the seismic noise spectra to changing meteorological conditions. Progressively stronger winds and the ensuing larger surface gravity waves result in a migration toward lower-frequency, higher-energy microseisms. Also of interest are the relative power levels of the different size storms. For the nor'easter, the largest meteorological event, the power levels reached are much greater and the frequencies at maximum power are lower as compared to the smaller storms. Obviously, meteorological conditions (especially wind velocity) play a key role in controlling the excitation of microseismic noise. Although we only discussed a few storms of many, these same characteristics are also apparent in the other storms observed over the experimental period.

Other interesting features revealed in Figure 10 are the low-frequency peaks of the double-frequency peak near 0.18 Hz, which are not associated with local storm activity but instead are connected with distant storms.

Here, the low-frequency microseisms are generated at the source (distant storm) and propagate to the receiver. During the locally quiet meteorological period, the apparently teleseismic event (near day 306) shows the same frequency and power level characteristics associated with the onset of a storm. The fact that much lower frequencies are excited means that this event is probably associated with a very large storm covering several hundred kilometers. Only large (and, hence, rare and usually distant) storms will generate the lowest-frequency microseisms (Webb, 1992). For distant storms, the amount of microseism energy ultimately depends on the lateral extent or fetch of the source region. (Measurements of microseism activity for local events depend upon the distance from the experimental site to the outward edge of the storm or source region.) Though uncommon in the Atlantic, microseisms at frequencies below about 0.14 Hz [corresponding to ocean waves of 0.07 Hz and sustained wind velocities of more than 20 m/sec in the previously described Pierson and Moskowitz (1964) model]

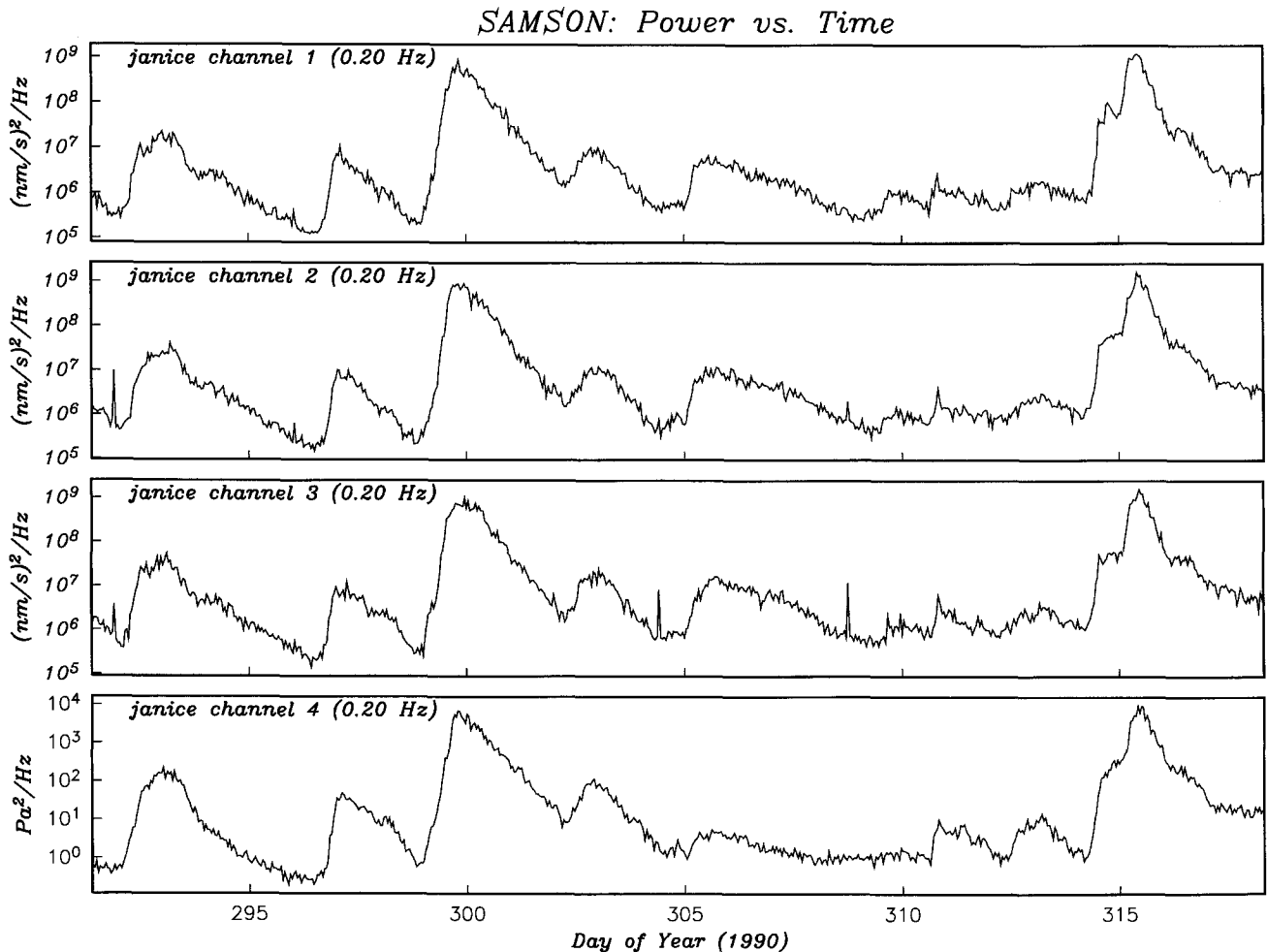


Figure 8. Comparisons between the three inertial components [channels 1 (vert.), 2 (horiz. 1), and 3 (horiz. 2)] and the hydrophone (channel 4) at 0.20 Hz for Janice.

require a fetch on the order of 600 km or more to reach a fully developed sea state (Webb, 1992).

Figure 11 shows a “sonogram” of a different perspective for Janice’s hydrophone and, again, gives a spectral history for the entire experiment. This representation is much better at showing the shape of individual spectral estimates, as opposed to the power levels shown in the previous contoured plot. Here, the bifurcation in the double-frequency peak, due to local and teleseismic events, is more evident. Though meandering slightly in frequency at times, distant microseism activity generally seems to “lock” to a preferential frequency (near 0.18 Hz) and the bandwidth tends to be quite narrow. As microseism energy travels away from the source region, the spectrum attenuates, with the highest frequencies lost first, while the lower frequencies persist. This selective attenuation of higher frequencies, possibly exaggerated by thick sediment layers that are typical for the Atlantic, and the lower-frequency bound, determined by the overall fetch of the storm (which controls the longer-period surface gravity wave interactions), result in a sharp appearance

of the teleseismic peak. The peaking is further enhanced by Rayleigh mode resonance, resulting in higher amplitude levels. Following the climax of storm development, the teleseismic peak also reveals an evolution with time toward a higher frequency, suggesting normal dispersion of seismic waves from a distant source (Webb and Cox, 1986). In fact, this trend is more likely due to the dissipation of the storm rather than dispersion. As the storm reaches its peak (where excitation and dissipation are equal), and begins to decline, there is a gradual reduction in amplitude and period associated with a dissipating storm. This characteristic is also shown in local storm activity for both the SAMSON (i.e., the nor’easter in Figs. 10 and 11) and Maui (to be discussed) experiments.

#### Relevant Studies

In their Maui experiment in the Cook strait off the coast of New Zealand (where both environmental parameters in shallow water and nearby land measurements of microseismic excitation were recorded), Kibblewhite and

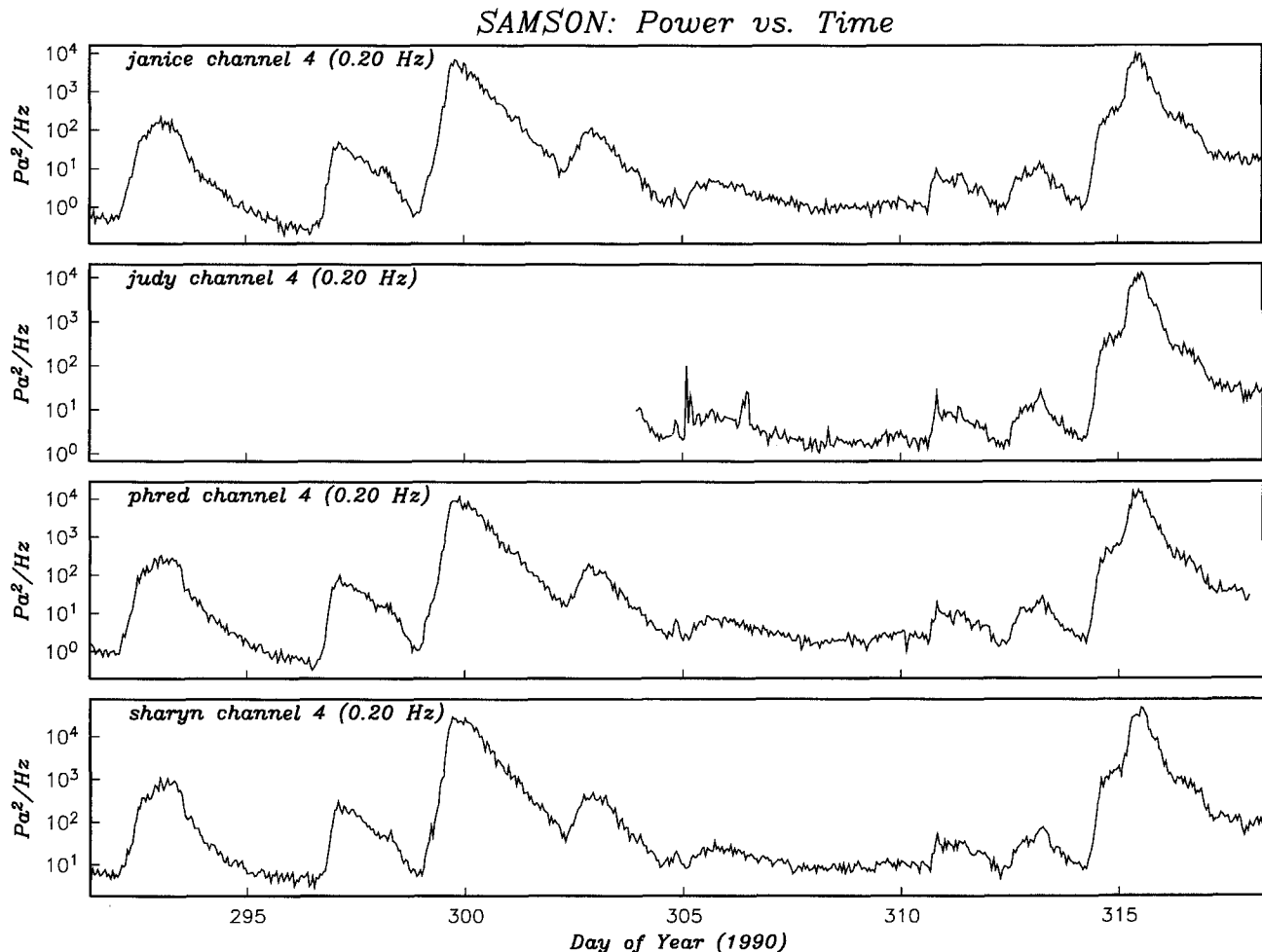


Figure 9. The hydrophone channels of the four operating OBS’s at 0.20 Hz show very similar amplitudes and shapes.

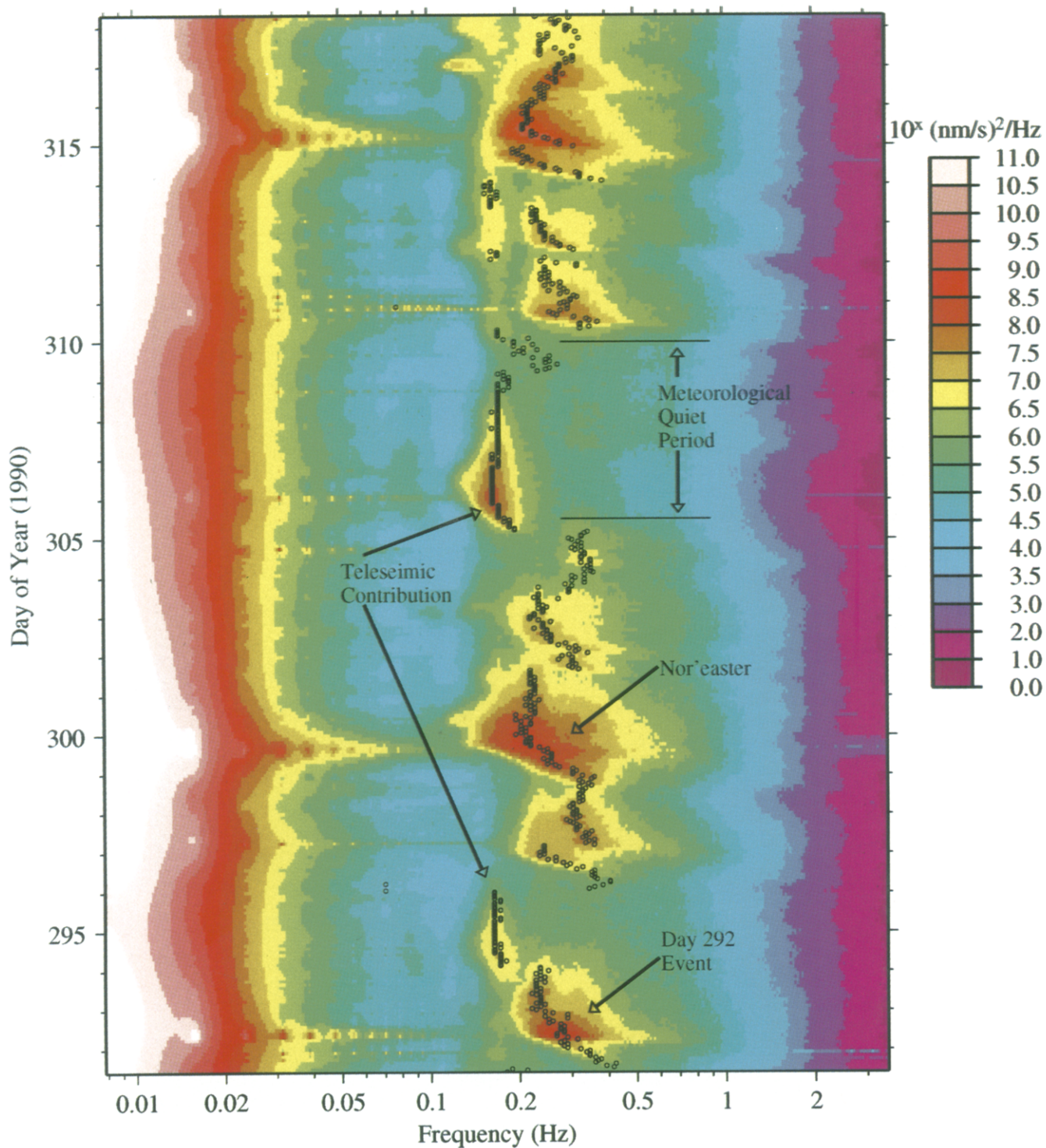


Figure 10. The power spectrum for the vertical seismometer of Janice over the entire experiment. The small black circles represent the frequency at which the maximum power level occurs in the microseism peak. The temporal response due to the passage of a storm is clearly evident as a decrease in peak frequency along with an increase in amplitude. Contours indicate exponential power levels in  $(\text{nm}/\text{sec})^2/\text{Hz}$ .

Ewans (1985) show similar results over an extended experimental time period. The temporal response due to the passage of a storm shows a remarkable resemblance to those seen in SAMSON results. This is not entirely unexpected, since the mechanisms for the generation of double-frequency microseism noise work equally as well for both shallow or deep water. Subtle differences, how-

ever, do occur when comparing shallow and deep water results. For example, though sustained winds of over 30 m/sec were reached in the Maui experiment, significant wave heights above 6 m were infrequent. A comparison with SWADE data reveals wave heights of nearly 8 m in only 20 m/sec winds. This can be attributed to the limited fetch, attainable because of the proximity of the

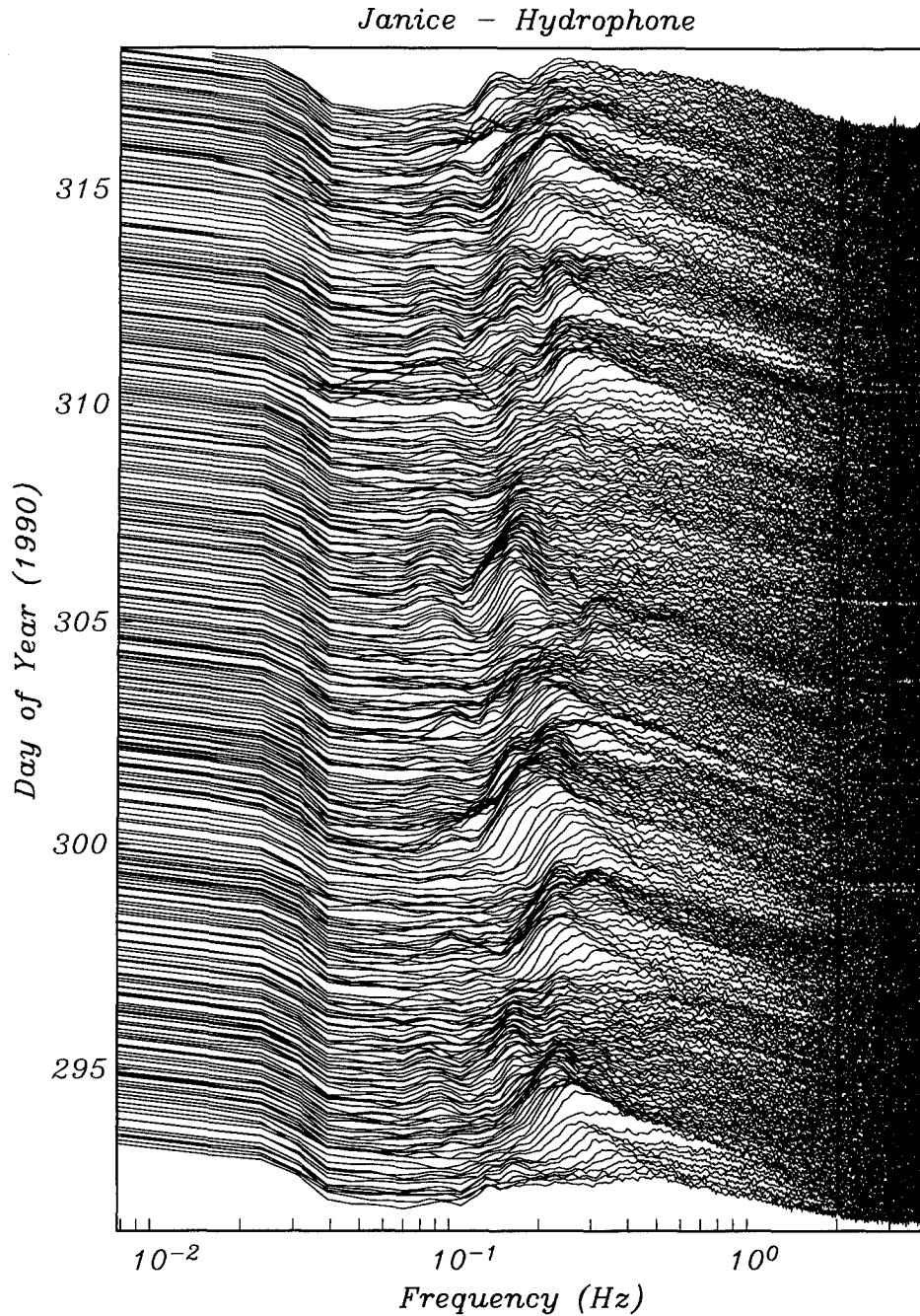


Figure 11. A "sonogram" showing individual spectral estimates for Janice's hydrophone. The general shape of individual spectral estimates is better represented. For better resolution, every other hour is plotted and subsequent spectra are slightly offset. Amplitude levels are similar to those shown in Figure 4. The elevated amplitudes seen at 2 and 3 Hz are the result of an anomalous glitch in the OBS data.

coastline and dissipation in the shallow water setting near New Zealand. Though the variability of the pressure spectra for microseisms in shallow water can vary drastically, Webb (1992) calculations for equilibrium microseism results show that the displacement spectra are smaller by 20 dB for shallow as compared to deep water (comparing water depths of 500 and 5000 m, respectively).

Deep ocean studies in the Pacific also reveal similar results in response to the passage of a storm. Pressure studies in 1.6-km-deep water done by Webb and Cox (1984) portray a spectral shoulder, evolving from higher frequencies near 0.7 Hz down to 0.25 Hz, along with a concurrent increase in intensity. Frequency and power shifts are associated with the sudden onset of strong wind with an increase in wind speed from 12 to 20 m/sec and a change in wind direction of 90°. These observations are consistent with the nonlinear, double-frequency interference mechanism described by Hasselmann (1963) and Cox *et al.* (1978).

#### Nonpeak Observations

As in the Pierson and Moskowitz (1964) model of ocean wave spectra and in the closely related models of microseism spectra (e.g., Webb, 1992), the power spectral levels associated with the higher frequencies tend to be saturated. Though slightly elevated noise levels associated with the larger storms are apparent, frequencies greater than 2 Hz reveal only minor deviations in amplitude levels with time (see Fig. 10). Somewhat unexpectedly, in the noise notch, elevated amplitudes occur in conjunction with several of the larger storms. Though suggestions have been made that this might be an artifact of spectral leakage, this appears to be highly unlikely, based on experiments with multi-taper spectra designed to limit such leakage. A possible explanation could be the direct radiation of atmospheric turbulence, causing higher noise levels (Guo, 1987). Also surprising is the presence of a response in the ultra-low frequency (ULF) band. The 1-Hz natural period sensor used on the OBS's effectively has a useful response down to roughly 0.08 Hz (Willoughby *et al.*, 1993), yet signals are still seen at very low frequencies. The fact that a reasonable signal can be observed is due to the large-scale averaging in spectral estimates, which provides enough spectral stability and noise reduction to resolve long-term variations. The same ULF variations are observed on the broadband pressure channel.

#### Single Frequency Peak

The waterfall plot (Fig. 11) also reveals a much lower-amplitude single or primary frequency peak that is roughly centered at 0.09 Hz. Note the continuity of this feature throughout the experiment. Conditions in which local winds exceed roughly 10 m/sec lead to sufficient frequency migration of the local double-frequency peak to

mask the single-frequency peak, but otherwise it is present. Spectral estimates from several island sites in the Pacific Ocean reveal a wide variability in the amplitude and shape of single-frequency microseisms (Hedlin and Orcutt, 1989). This contrasts with observations in continental data, where single-frequency microseisms are commonly observed with much higher relative power levels (Lacoss *et al.*, 1969; Murphy and Savino, 1975), as compared to oceanic measurements.

Observing the single-frequency peak in the Pacific is much more difficult than in the Atlantic because it is often masked by the larger-amplitude, lower-frequency double-frequency peak associated with bigger "Pacific" storms. This makes the Atlantic a more ideal setting for the study of single-frequency microseisms. It has been proposed (Lahav, 1991) that the generation of the single-frequency peak in the Pacific is due to teleseismic earthquakes. During Julian day 310 of the SAMSON experiment, a teleseismic earthquake of magnitude 6.3 occurred at ~20:14 near the Aleutian Trench in Alaska. However, the *P*-wave arrival and the subsequent Rayleigh wave train affect the entire noise notch (0.02 to 0.1 Hz) of the microseism band and is not seen as a single-frequency peak but rather as an overall broadband biasing. (The effect of the teleseismic earthquake is easier to see in Fig. 11.) The long duration of the single-frequency peak and the lack of very many moderate to large earthquakes during the recording period make it unlikely that teleseismic earthquake activity could be the cause of single-frequency microseism excitation.

Of particular interest is how the primary peak tends to "mirror" any meanders in frequency of the teleseismic double-frequency peak. Comparison of the two peaks from quiet days 305 through 308 gives a good example of this behavior (see Fig. 11). Characteristics observed are quite similar to those seen in local storm activity; during the excitation of the distant storm, both peaks show a concurrent progression from higher to lower frequencies, as well as an increase in magnitude. As the storm dissipates, there is a trend from lower to higher frequencies, along with a decrease in power levels. These effects would be consistent with the formation of the peaks from the same storm. Coherence studies confirm the propagation of single-frequency microseisms from a distant source. Though studies in the Pacific (Webb and Constable, 1986) suggest that the primary peak source is at a different location than the double-frequency source, it cannot be concluded that both peaks must be generated at different locations. For the SAMSON experiment, it is unlikely that the production of the two peaks could occur in different locations and still show the same temporal, frequency, and power characteristics. In fact, the distant storm producing this observed energy would have to be located near the coastline, since the energy associated with the single-frequency peak is excited in shallow water

where the mechanisms for excitation of double-frequency peak values are equally valid. We note, however, that the mechanism for exciting the single-frequency microseisms is poorly understood. The phase velocities associated with surface gravity waves acting on the seafloor in shallow water are too low to excite seismic waves. Nonlinear effects such as breaking waves on a shoreline must be responsible for single-frequency excitation.

#### Coherence Studies

Figure 12 plots the coherence between the hydrophones of instruments Janice and Phred (4.3 km apart) in the frequency band of  $\sim 0.008$  to 4 Hz during the SAMSON deployment. The single-frequency peak coherence band is centered on 0.09 Hz and the teleseismic double-frequency peak coherence occurs in the vicinity of 0.18 Hz. Local generation of the noise wave field by meteorological interactions at the ocean surface results in random pressure gradients in the seafloor pressure field, thereby producing an inhomogeneous wave field. This results in low coherence values for the local contribution to the double-frequency microseism peak. Only when the source is at large distances can the resultant wave field be adequately collimated to be coherent. High coherence in the single- and teleseismic double-frequency peaks frequently occurs simultaneously, again suggesting that the primary peak is teleseismic and is created at the same time and general location as the teleseismic double-frequency peak. (Though not shown, coherence values for the seismometer components reveal that the double-frequency coherence is highest at times of low local meteorological activity.) Instantaneous coherence of the single-frequency peak reaches values as high as 0.78, indicating a well-collimated teleseismic source.

As expected, the distant earthquake during day 310 (previously described), which gives elevated spectral levels in the noise notch, is also associated with higher coherence values (see Figs. 11 and 12). Similarly, the high coherence levels observed in the noise notch near day 300 are thought to come from the combination of a distant and regional pair of events. On 27 October (day 300) at  $\sim 12:47$  there was a magnitude 5.2 earthquake approximately 2000 km from the OBS array in the Leeward Islands. Also, at  $\sim 13:12$  the same day, the data reveal a much smaller regional earthquake several hundred kilometers from the array. Amplitudes of the incoming propagating waves could be low enough to avoid detection in spectral estimates but sufficiently well collimated to cause higher coherence values. Several other small (coherent) seismic events can also be observed between days 292 and 300 in Figure 12.

#### Array Studies

From complex coherence, several properties of the seismic waves under study can be determined. Primar-

ily, the propagation origin and velocity can be studied using beamforming methods. Given the sparseness of the array and significant sidelobes calculated for the seafloor array impulse response, we elected to use the beamforming method of maximum entropy or maximum likelihood (Capon, 1969). This method seeks to localize the energy in wavenumber ( $\mathbf{k}$ ) space for improved resolution. Figure 13 is the maximum entropy beamforming result during a period when the teleseismic double-frequency peak coherence was high (0.188 Hz), on day 311. In this contour plot, the azimuthal direction of propagation is indicated by two energy peaks; however, only one peak represents the source. The outer circle represents phase velocities of 1500 m/sec and the inner circle 4500 m/sec. Since we propose that the double-frequency peak is teleseismic, and we know that (1) the seafloor array location is very near the North Carolina coast, and (2) teleseismic microseism components are absent in shallow water observations because of the inhomogeneous wave field (Kibblewhite and Wu, 1991; Kibblewhite and Ewans, 1985), we chose the northeast direction as the origin. The velocity of the double-frequency peak,  $r = 0.88$  or about 1700 m/sec (0.188 Hz), constrains this wave to propagate largely within the water column. If the southwest direction were correct, the double-frequency wave must propagate through continental North America at 1700 m/sec—an unrealistically low velocity. Based on this velocity and direction of origin, it would appear as if the majority of microseismic energy propagates within the water column in the Atlantic Ocean. Webb (1992) reports in a Pacific Ocean study that observed microseisms propagate at 4500 m/sec, which implies that a majority of the energy is propagating in the oceanic lithosphere. Thus, in contrasting the results from SAMSON in the Atlantic Ocean to those of Webb in the Pacific, there does not yet appear to be a consistent mode of propagation for microseisms.

#### Conclusions

The double-frequency microseism peak is a very clear and ever-changing feature in Atlantic seafloor noise spectra. Bifurcated at times, this peak contains local and teleseismic components that are generated at different locations. Weather and storm fetch appear to be the major contributors to the size and shape of microseism spectra. Based upon the high correlation between wind speed, wave height, and the amplitude of double-frequency microseisms seen during local storm activity, it seems clear that nonlinear wave interaction must control ocean noise in this band. This is supported by the observation that changes in wind direction, which allow a more isotropic wave field and, therefore, more wave-wave interactions, are associated with greater noise levels.

Of particular interest in this experiment is the high variability of observed microseisms at this site, especially the high temporal variability in peak frequencies

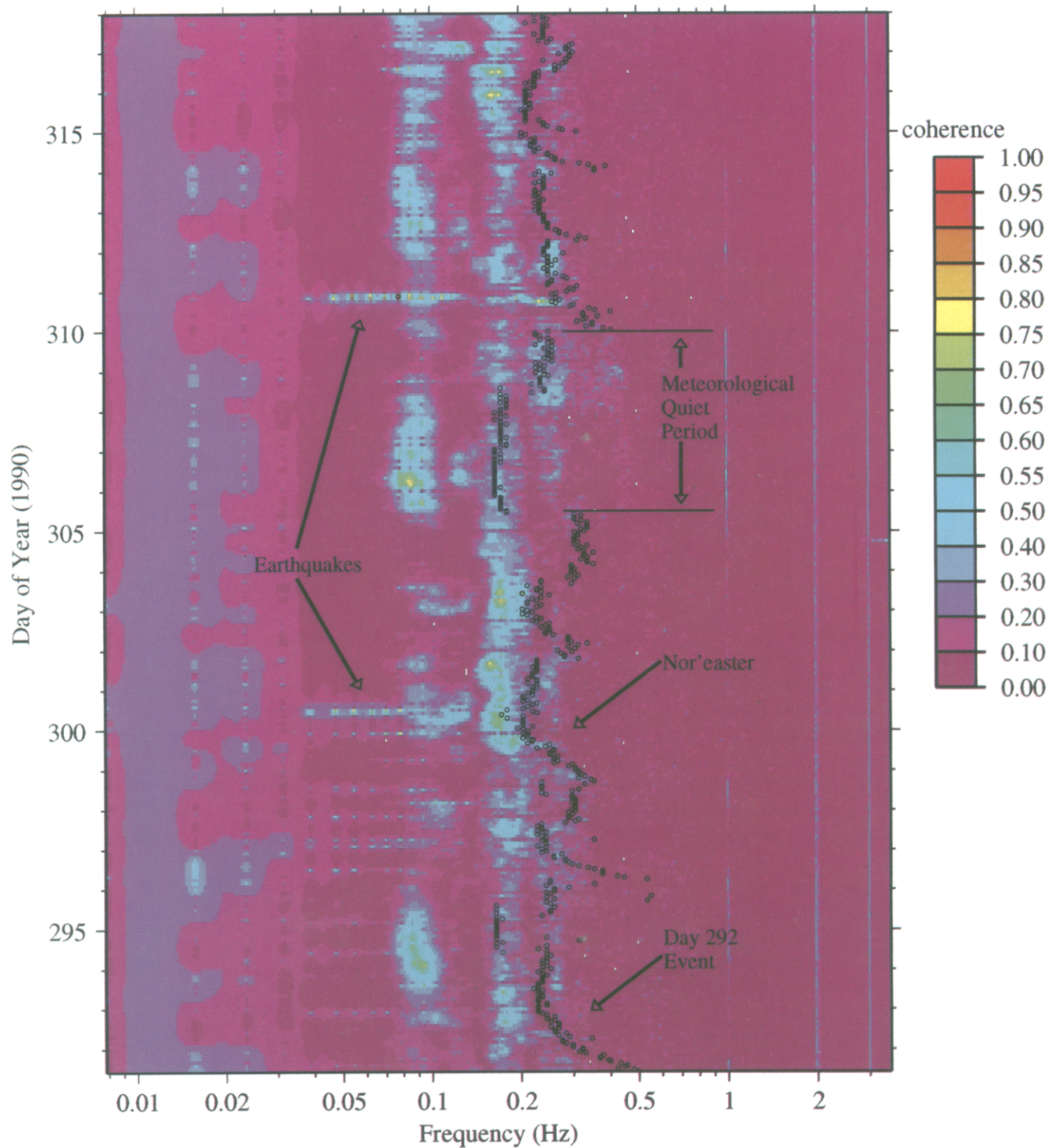


Figure 12. Coherence estimates between the hydrophones on instruments Jan-ice and Phred (4.3 km apart). The small black circles represent the frequency at which the maximum power occurs in the microseism peak from spectral calculations. The two distinct bands centered around 0.09 and 0.18 Hz are the single- and teleseismic double-frequency peaks, respectively.

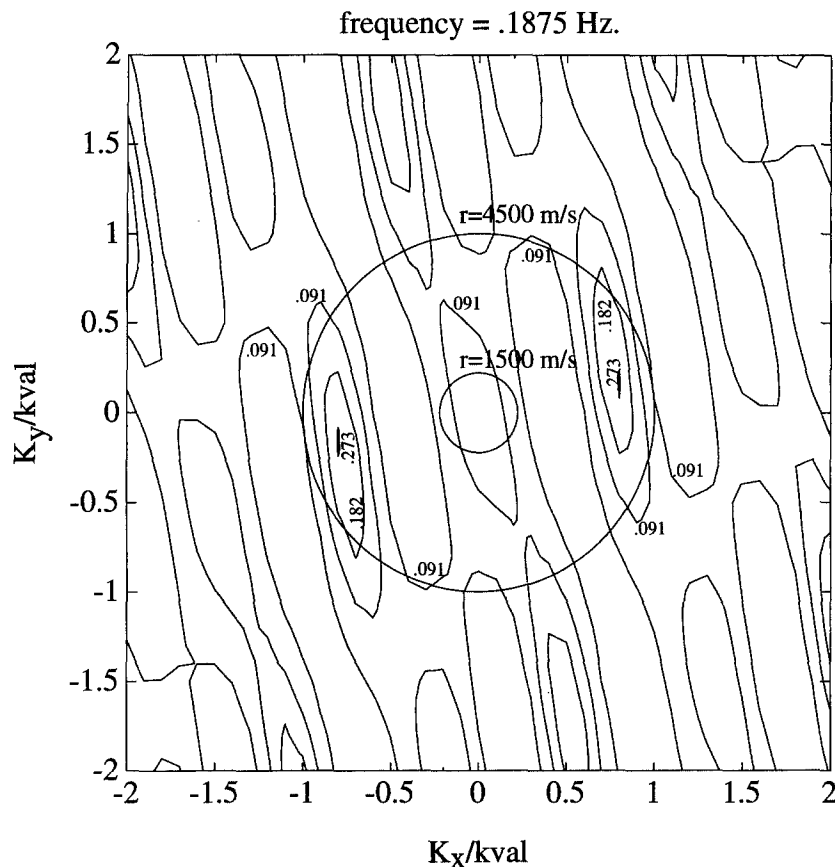


Figure 13. Maximum likelihood beam forming on the teleseismic double-frequency peak. The plot is shown in normalized wavenumber ( $\mathbf{k}$ ) space and contours indicate wave energy. Here the north direction is at the top and west is to the left, with energy peaks occurring in the northeast and southwest directions. The outer circle represents phase velocities of 1500 m/sec and the inner circle 4500 m/sec. The peak is at a circle radius of  $r = 0.88$  or about 1700 m/sec.

and the significant changes (over short periods) in microseism amplitudes. Excitation due to the passage of a storm consistently results in a distinct migration from higher to lower frequencies with a concurrent increase in power. This response is observed in both large and small storms that generate the local double-frequency peak, as well as in the single- and double-frequency peaks connected with teleseismic events. During large local storm activity, the local double-frequency microseism peak can overshadow the teleseismic portion of this band, while the elevated noise levels in the noise notch can mask the single-frequency peak.

The single-frequency microseism peak is a continuous feature observed during the SAMSON experiment. Earthquakes seem to play a minor role in primary frequency microseism excitation. Coherence studies suggest that the single- and teleseismic double-frequency microseisms are generated at the same time and location and require that some part of the storm extend over shallow water. Comparisons between Pacific and Atlantic array studies appear to indicate that there is no consistent mode of propagation for microseisms.

### Acknowledgments

We thank the officers and crew of the University of Rhode Island's R/V Endeavor for their excellent support at sea and for making the

SAMSON experiment a great success. This research was supported by ONR N000-90-J-1087. We thank Spahr Webb for helpful comments while we conducted this research.

### References

- Capon, J. (1969). High resolution frequency wavenumber spectrum analysis, *Proc. IEEE* **57**–**58**, 1408–1418.
- Cessoro, R. K. and W. W. Chan (1989). Wide-angle triangulation array study of simultaneous primary microseism sources, *J. Geophys. Res.* **94**, 15555–15563.
- Cox, C. S., N. Kroll, P. Pistek, and K. Watson (1978). Electromagnetic fluctuations induced by wind waves on the deep-sea floor, *J. Geophys. Res.* **83**, 431–442.
- Guo, Y. P. (1987). On sound generation by weakly nonlinear interactions of surface gravity waves, *J. Fluid Mech.* **181**, 311–328.
- Guza, R. T. and E. B. Thornton (1982). Swash oscillations on a natural beach, *J. Geophys. Res.* **87**, 482–491.
- Hasselmann, K. A. (1963). A statistical analysis of the generation of microseisms, *Rev. Geophys.* **1**, 177–210.
- Hasselmann, K., T. P. Barnett, E. Bouws, H. Carlson, D. E. Cartwright, K. Enke, J. A. Ewing, H. Gienapp, D. E. Hasselmann, P. Kruseman, A. Meerburg, P. Muller, D. J. Olbers, K. Richter, W. Sell, and H. Walden (1973). Measurements of wind-wave growth and swell decay during the Joint North Sea Wave Project (JONSWAP), *Dent. Hydrogr.* **2**, Supplement, A8.
- Haubrich, R. A. and K. McCamy (1969). Microseisms: coastal and palagic sources, *Rev. Geophys.* **7**, 539–571.
- Hedlin, M. A. H. and J. A. Orcutt (1989). A comparative study of island, seafloor, and subseafloor ambient noise levels, *Bull. Seism. Soc. Am.* **79**, 172–179.

- Kibblewhite, A. C. and K. C. Ewans (1985). Wave-wave interactions, microseisms and infrasonic ambient noise in the ocean, *J. Acoust. Soc. Am.* **78**, 981–994.
- Kibblewhite, A. C. and C. Y. Wu (1991). The theoretical description of wave-wave interactions as a noise source in the ocean, *J. Acoust. Soc. Am.* **89**, 2241–2252.
- Lacoss, R. T., E. J. Kelly, and M. N. Toksöz (1969). Estimation of seismic noise structure using arrays, *Geophys.* **34**, 21–38.
- Lahav, D. (1991). Observations of low frequency ambient signals in the deep ocean, *Master's Thesis*, University of California, San Diego, La Jolla, California.
- Longuet-Higgins, M. S. (1950). A theory of the origin of microseisms, *Philos. Trans. R. Soc. London* **A243**, 1–35.
- Munk, W. H. (1949). Surf. beats, *EOS* **30**, 849–854.
- Murphy, A. J. and J. M. Savino (1975). A comprehensive study of long-period (20–200 seconds) earth noise at the high-gain worldwide seismograph stations, *Bull. Seism. Soc. Am.* **65**, 1827–1862.
- Oppenheim, A. V. and R. W. Schaffer (1975). *Digital Signal Processing*, Prentice-Hall, Englewood Cliffs, New Jersey, 556.
- Orcutt, J. A., C. S. Cox, A. C. Kibblewhite, W. A. Kuperman, and H. Schmidt (1993). Observations and causes of ocean and seafloor noise at ultra-low and very-low frequencies, in *Natural Physical Sources of Underwater Sound*, Kluwer Academic Publishers, Norwell, Massachusetts, 203–232.
- Pierson, W. J. and L. Moskowitz (1964). A proposed spectral form for fully developed wind seas based on the similarity theory of S. A. Kiaigorodskii, *J. Geophys. Res.* **69**, 5181–5190.
- Schreiner, A. E. and L. M. Dorman (1990). Coherence lengths of seafloor noise: effect of ocean bottom structure, *J. Acoust. Soc. Am.* **88**, 1503–1514.
- Symonds, G., D. A. Huntley, and A. J. Bowen (1982). Two dimensional surf beat: long wave generation by a time-varying breakpoint, *J. Geophys. Res.* **87**, 492–498.
- Tucker, M. J. (1950). Surf beats: sea waves of a 1 to 5 minute period, *Proc. R. Soc. London* **A207**, 565–573.
- Webb, S. C. (1988). Long-period acoustic and seismic measurement and ocean floor currents, *IEEE J. Ocean Eng.* **13**, 263–270.
- Webb, S. C. (1992). The equilibrium oceanic microseism spectrum, *J. Acoust. Soc. Am.* **92**, 2141–2158.
- Webb, S. C. and S. C. Constable (1986). Microseism propagation between two sites on the deep ocean floor, *Bull. Seism. Soc. Am.* **76**, 1433–1455.
- Webb, S. C. and C. S. Cox (1984). Pressure and electric fluctuations on the deep seafloor: background noise for seismic detection, *Geophys. Res. Lett.* **11**, 967–970.
- Webb, S. C., and C. S. Cox (1986). Observations and modeling of seafloor microseisms, *J. Geophys. Res.* **91**, 7343–7358.
- Willoughby, D. F., J. A. Orcutt, and D. Horwitt (1993). A micro-processor based ocean-bottom seismometer, *Bull. Seism. Soc. Am.* **83**, 190–217.

Institute of Geophysics and Planetary Physics  
Scripps Institution of Oceanography  
La Jolla, California 92093-0225

Manuscript received 13 October 1993.